Journal of Applied Physics

Measurement of magnetic anisotropy constant for magneto-optical recording media: A comparison of several techniques

Cite as: Journal of Applied Physics **73**, 1368 (1993); https://doi.org/10.1063/1.353256
Submitted: 24 July 1992 . Accepted: 09 October 1992 . Published Online: 04 June 1998

Te-ho Wu, Hong Fu, R. A. Hajjar, T. Suzuki, and M. Mansuripur

Measurement of magnetic anisotropy constant for magneto-optical recording media: A comparison of several techniques

Te-ho Wu and Hong Fu
Optical Sciences Center, University of Arizona, Tucson, Arizona 85721

R. A. Hajjar
Eastman Kodak Company, Rochester, New York 14652

T. Suzuki
IBM Research Division, Almaden Research Center, San Jose, California 95120

M. Mansuripur
Optical Sciences Center, University of Arizona, Tucson, Arizona 85721

(Received 24 July 1992; accepted for publication 9 October 1992)

Experimental data of the intrinsic perpendicular magnetic anisotropy energy constant K_u are presented for amorphous rare earth-transition metal (RE-TM) $Tb_x(FeCo)_{1-x}$ and multilayered Co/Pt thin film samples. These data were independently measured using five techniques based on torque magnetometry, the extraordinary Hall effect, and the magneto-optic Kerr effect. In the Hall effect measurement, the external field was applied to the sample in three different ways: fixed at 45° from the film normal; rotating around the sample; and fixed along the in-plane direction. The results obtained with these techniques agree with each other for the Co/Pt samples. However, we do find systematic differences in the measured K_u for the $Tb_x(FeCo)_{1-x}$ samples. For example, K_u given by the Hall effect and Kerr effect is always larger (by up to a factor of 3) than that given by torque technique. Another interesting fact is that K_u given by the Hall effect technique drops as x approaches the compensation point x_c in the TM-dominant case, but increases as x approaches x_c in the RE-dominant case. These experimental results are explained by taking into account the canting between RE and TM subnetworks.

I. INTRODUCTION

The perpendicular magnetic anisotropy energy constant K_u is an important property of the magneto-optical recording media. Measurement of K_u has been the subject of many investigations. The purpose of the present article is to compare several techniques which have been frequently used in measuring K_u for magneto-optical recording media. Such a comparison is necessary because often different techniques give different results. The differences in the measured K_u stem from the different micromagnetic processes involved.

The article is organized as follows. The various techniques employed in this work are described in Sec. II. The experimental data of K_u for four amorphous $Tb_x(FeCo)_{1-x}$ and two multilayered Co/Pt thin film samples are presented in Sec. III. These data show that the value of K_u obtained for $Tb_x(FeCo)_{1-x}$ samples depends on the technique utilized, while for Co/Pt samples all the techniques give the same result. In Sec. IV, we interpret the differences for $Tb_x(FeCo)_{1-x}$ samples based on the canting between the RE and TM subnetwork magnetizations. Concluding remarks are presented in Sec. V.

II. DESCRIPTION OF THE TECHNIQUES

A. Stoner–Wohlfarth model—the theoretical basis

The measured anisotropy constant K_u is commonly deduced from the experimental data based on the Stoner–Wohlfarth (SW) model[1,2] under the assumption of the coherent magnetization rotation. In this model the total magnetic energy density of the film is written (see Fig. 1),

$$E_{\text{tot}} = -HM_s\cos(\alpha-\Theta) - 2\pi M_s^2\sin^2\Theta + K_u\sin^2\Theta, \tag{1}$$

where the three terms are the external field energy, the demagnetizing energy and the uniaxial anisotropy energy, respectively. In general, the uniaxial anisotropy energy has the form $K_{u1}\sin^2\Theta + K_{u2}\sin^4\Theta + \cdots$, but we found that the first term is sufficient to match the experimental data for our samples. In the experiment, H and α are known, and one measures essentially M_s and Θ, using different techniques, e.g., torque magnetometry, the magneto-optical Kerr effect, or the extraordinary Hall effect. With H, α, M_s, and Θ known, one can find K_u from the energy minimum condition, namely,

$$\frac{\partial E_{\text{tot}}}{\partial\Theta} = -HM_s\sin(\alpha-\Theta) + (K_u - 2\pi M_s^2)\sin(2\Theta) = 0. \tag{2}$$

To get higher accuracy, one usually measures a series of data with varying H or α, and then uses the SW solution to best fit the curve by adjusting K_u.

B. The techniques

1. Torque magnetometry with the field at 45°

This technique was developed by Miyajima *et al.*[3] It consists of applying a magnetic field H at 45° to the film normal and measuring the torque L. Using L

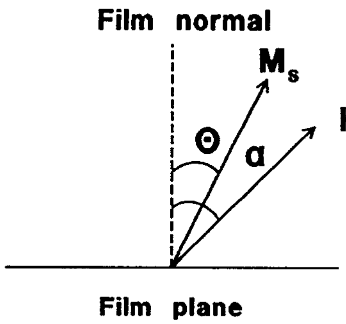

FIG. 1. Definitions of the angles α and Θ for the applied field **H** and the magnetization **M** relative to the film normal.

$= HM_s \sin(45°-\Theta)$, Eq. (2) can be written as $(L/H)^2 = 0.5\ M_s^2\ [1-L/(K_u-2\pi M_s^2)]$. Therefore, by plotting $(L/H)^2$ vs L, one can find M_s and K_u from the intercept and the slope of the straight line passing through the experimental data.[3-6] One advantage of this method is that K_u and M_s can be obtained simultaneously.

2. Techniques based on Hall effect and Kerr effect

For a magnetic thin film the extraordinary Hall voltage and the magneto-optical polar Kerr rotation angle are proportional to the perpendicular component M_z of the magnetization **M**.[7-9] By properly normalizing the Hall/Kerr signal to the height of the hysteresis loop and taking the inverse cosine of the normalized value, we can find the angle Θ of **M** as a function of the magnitude H and direction α of the applied field, i.e., $\Theta=\Theta(H,\alpha)$. The saturation magnetization M_s can be measured by the vibrating sample magnetometer (VSM) or by torque measurement.

In the Hall effect measurement the ordinary Hall effect produced by the applied magnetic field must be eliminated. For the $Tb_x(FeCo)_{1-x}$ and Co/Pt samples studied in this article, the ordinary Hall effect is usually less than 1% of the measured signal. However, the change of the ordinary Hall signal during the measuring process (due to the change of the external field) can constitute a significant portion in the variation of the total signal, from which K_u is derived. This is especially true for samples near the compensation point, where the magnetization can only be slightly tilted because of the large anisotropy field, and the ordinary Hall effect can be dominant in the measured signal variations. We use the following method to eliminate the ordinary Hall effect. The measured Hall signal S is contributed by both extraordinary Hall effect S_e and ordinary Hall effect S_o, i.e., $S=S_e(M_s \cos\Theta)+S_o(H\cos\alpha)$, where S_e is proportional to M_z or $\cos\Theta$, and S_o to the perpendicular component of the applied field. To deduce Θ for given α and H, we basically need three signals: the signal under zero field $S_1=S_e(M_s)$; the signal under a perpendicular field of magnitude $H\cos\alpha$, which is equal to $S_2=S_e(M_s)+S_o(H\cos\alpha)$; and the signal under the desired field (with magnitude H and angle α) which is $S_3=S_e(M_s\cos\Theta)+S_o(H\cos\alpha)$. With these signals, the tilted angle Θ can be found from the equation $\cos\Theta=S_e(M_s\cos\Theta)/S_e(M_s)=(S_3+S_1-S_2)/S_1$. In measuring $\Theta(H,\alpha)$, one can either change α or H, which leads to the following techniques:

Measuring Hall effect with 45° external field: The function $\Theta(H,\alpha=45°)$ is obtained by applying a 45° field and measuring the Hall voltage. In this technique the ordinary Hall effect must be eliminated from the measured signal. Although the torque is not measured directly, one can deduce it from the relation $L=HM_s\sin(45°-\Theta)$ (with M_s measured by VSM), and then find K_u in a similar way (plotting L^2/H^2 vs L) as in the 45° torque measurement. Figure 2 shows the procedure of extracting K_u for a $Tb_{30.3}(FeCo)_{79.7}$ sample using this technique. Figure 2(a) displays the measured signal as a function of the magnitude of the external field applied at 45° to the film normal. The signal variation contains both extraordinary and ordinary Hall effects. Figure 2(b) displays the measured signal when the field is perpendicularly applied to the sample. In this case the signal variation is contributed only by the ordinary Hall effect. Figure 2(c) shows the extraordinary Hall effect signal ($\cos\Theta$) obtained by properly eliminating the ordinary Hall effect contribution from Fig. 2(b). From Fig. 2(c) we can find Θ and hence L. The calculated L as a function of H is shown in Fig. 2(d). In Fig. 2(e) we see that the data points $(L/H)^2$ vs L form a straight line. The crossing of the straight line at the vertical axis is equal to $0.5\ M_s^2$, and the slope is equal to $-0.5\ M_s^2/(K_u-2\pi M_s^2)$, from which one finds K_u.

Measuring Hall effect with rotating field:[9] In this method we measure $\Theta(H,\alpha)$ by rotating the external field (with fixed magnitude H) around the sample from $\alpha=0°$ to 90° while monitoring the Hall voltage. The ordinary Hall effect must be removed from the measured signal.

Measuring Hall effect with in-plane external field[7,9]: In this technique we deduce the magnetization direction $\Theta(H,\alpha=90°)$ by measuring the Hall voltage versus the magnitude of the field **H** applied along an in-plane direction. One advantage of this technique is that, since the applied field is in-plane, there is no contribution from the ordinary Hall effect.

Measuring Kerr effect with in-plane external field:[7,8] In this technique we deduce the magnetization direction $\Theta(H,\alpha=90°)$ by measuring the Kerr rotation angle θ_k (proportional to $\cos\Theta$) versus the magnitude H of the field applied along an in-plane ($\alpha=90°$) direction. The wavelength of the laser beam used in the Kerr rotation measurement is 632 nm.

It is worth pointing out that the techniques using different external fields have some differences. For example, in the 45° field techniques, the tilted angle of the magnetization vector is usually small, because the field itself is 45° (not too much) tilted from the film normal direction. In the in-plane field techniques, the field does have the maximum tilted angle, but the magnetization rotation of the sample (especially the Co/Pt samples) may become incoherent as the field is increased to certain thresholds.[9,10] The coherent rotation angle of the magnetization vector may thus be limited. The rotating field technique provides the largest coherent rotation angle of **M**, because to some ex-

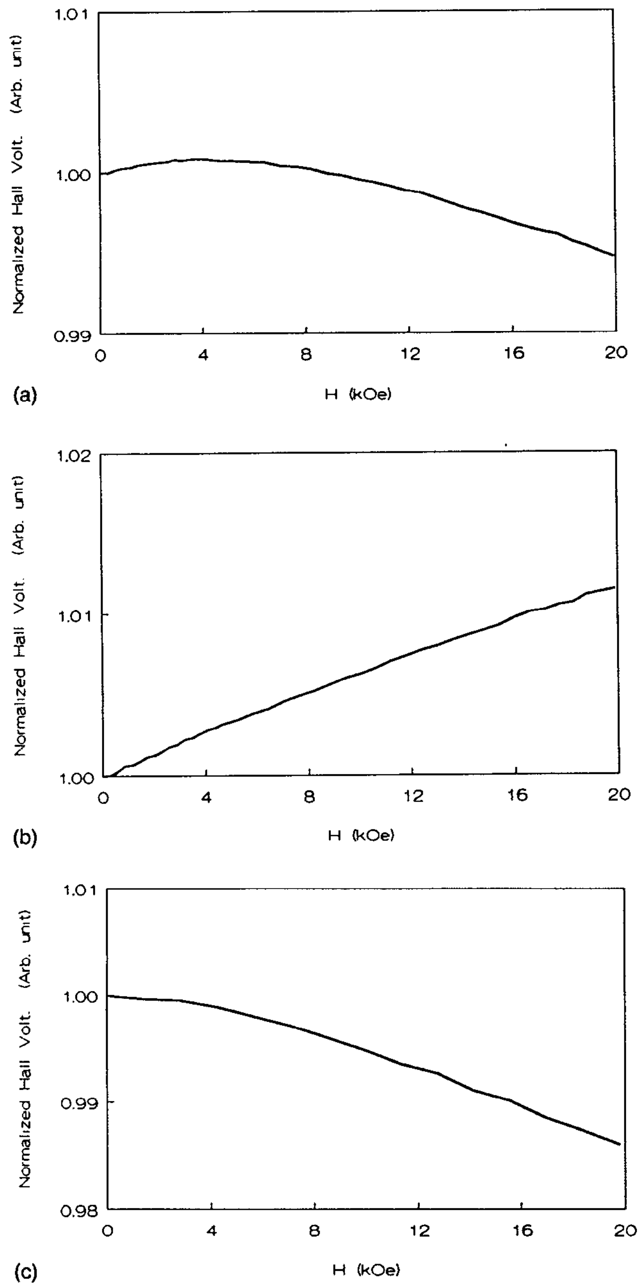

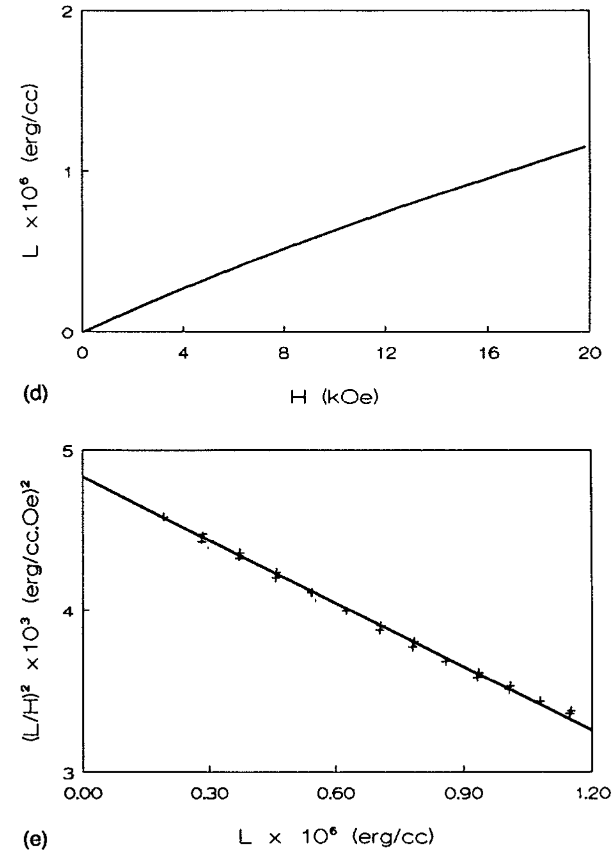

FIG. 2. Procedures in finding K_u from the experimental data in the 45° field/Hall effect technique. (a) The measured Hall voltage vs **H**, the magnitude of the 45° field. (b) The measured Hall voltage vs the magnitude of the perpendicularly applied field. (c) The extraordinary Hall signal ($\cos\Theta$) vs **H**, obtained by properly eliminating (b) from (a). (d) The calculated torque L vs **H**. (e) The data points in the L and $(L/H)^2$ plane forms a straight line, whose slope gives K_u.

tent the strong external field can prevent the film from demagnetizing. Therefore, the rotating technique offers a higher accuracy in the measured K_u. The extent of the coherent magnetization rotation is shown in Fig. 3 for a Co(3 Å)/Pt(10 Å) sample, where (a) corresponds to the 45° field technique ($\Theta_{max} \simeq 19°$), (b) represents the rotating field technique ($\Theta_{max} \simeq 45°$), and (c) corresponds to the in-plane field technique ($\Theta_{max} \simeq 37°$). The arrow in Fig. 3(c) marks the beginning of the incoherence.

The main difference between the Kerr effect and the Hall effect techniques is in the measured volume of the magnetic material. The Kerr signal is contributed by a small volume of the magnetic material which is located at the focus of the incident light (in the range of millimeters or smaller) and near the film surface (with a depth of a few hundred Å). Therefore, the K_u measured by the Kerr effect technique can fluctuate from one place to another, and is suitable for films of small thicknesses. One can make use of this feature to measure the spatial distribution of K_u. In contrast to the Kerr effect technique, the Hall effect signal is contributed by the entire sample, and the measured K_u thus reflects a "bulk" property.

III. EXPERIMENTAL OBSERVATIONS AND RESULTS

In this section we present the measured magnetic anisotropy energy constants K_u and some other magnetic properties for four amorphous $Tb_x(FeCO)_{1-x}$ and two multilayered Co/Pt thin-film samples. We use $K_u(45°/T)$, $K_u(45°/H)$, $K_u(\mathrm{Rot}/H)$, $K_u(90°/H)$, and $K_u(90°/\mathrm{K})$ to indicate the anisotropy energy constants measured by the aforementioned "45° field/torque," "45° field/Hall effect,"

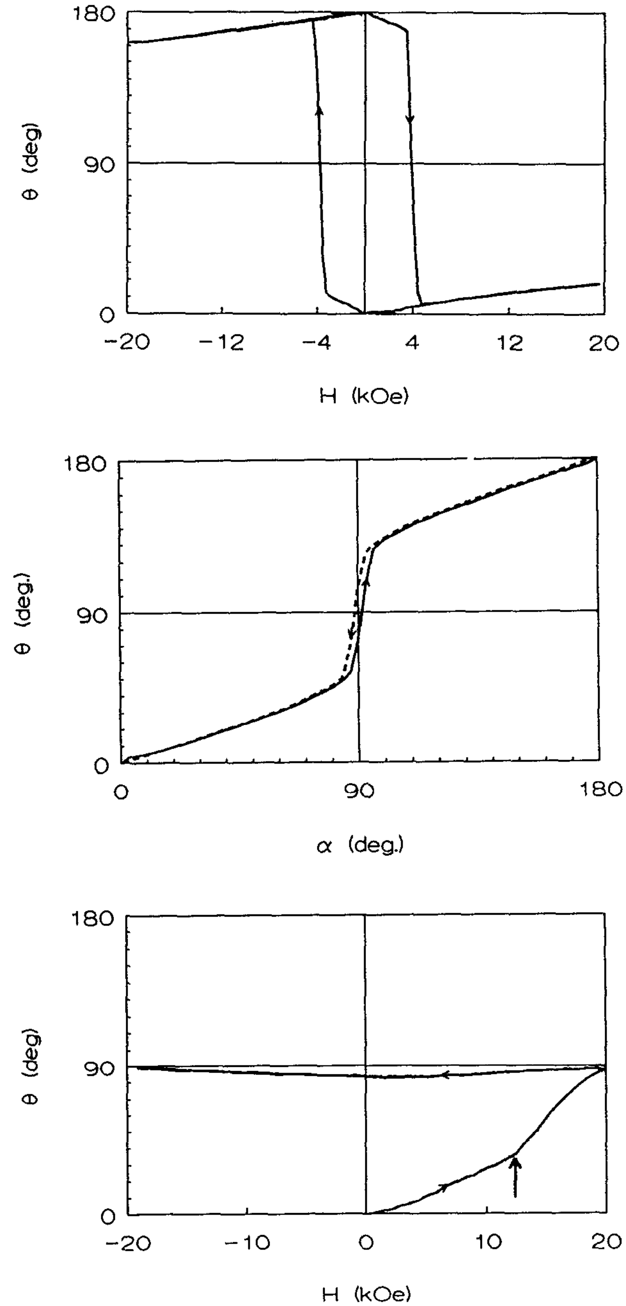

FIG. 3. The rotation angle of **M** in the different Hall effect techniques for the 260-Å-thick Co(3 Å)/Pt(10 Å) sample. (a) In the 45° field technique, the maximum coherent rotation angle $\Theta_{max} \simeq 19°$. (b) In the rotating field technique $\Theta_{max} \simeq 45°$. (c) In the in-plane field technique $\Theta_{max} \simeq 37°$. The arrow marks the beginning of demagnetization for larger **H**.

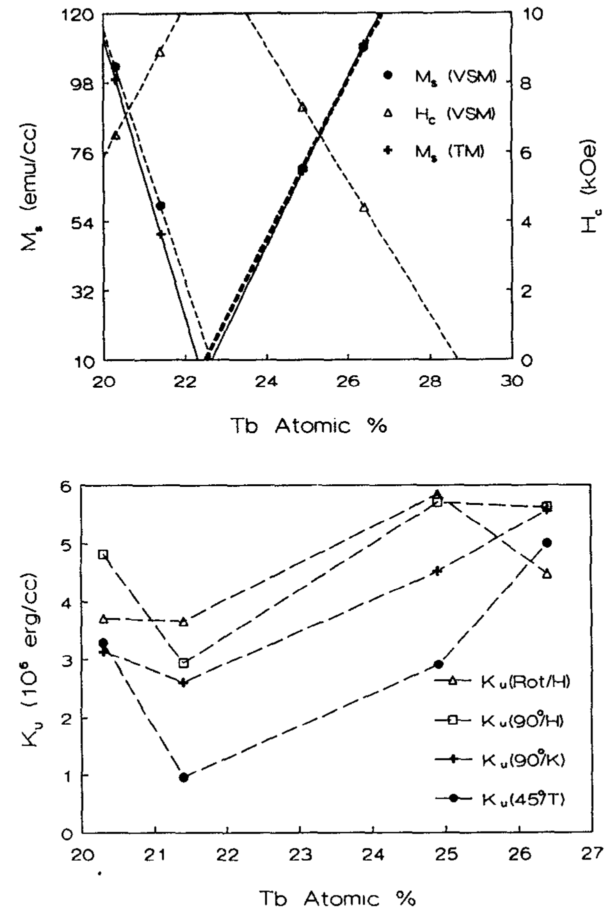

FIG. 4. The saturation magnetization M_s, coercivity H_c, and anisotropy constant K_u as functions of Tb content in amorphous $Tb_x(FeCo)_{1-x}$ thin films at room temperature. (a) M_s (●) and H_c (△) obtained from VSM, and M_s(+) obtained from the torque measurements. (b) The measured $K_u(45°/T)$ (●), K_u(Rot/H) (△), K_u(90°/H) (□), and K_u(90°/K) (+).

"rotating field/Hall effect," "in-plane field/Hall effect," and "in-plane field/Kerr effect" techniques.

The amorphous $Tb_x(FeCO)_{1-x}$ samples with $x=20.3\%$, 21.4%, 24.9%, and 26.4% are all 800 Å thick, sputter-deposited on glass substrates from an alloy target. The saturation magnetization of these samples was measured both with a VSM and with a torque magnetometer. The plot of M_s vs Tb content x in Fig. 4(a) shows a dip around $x_c=23\%$ which corresponds to the compensation composition at room temperature. The measured coercivity H_c shows a divergence around x_c, as expected for ferrimagnetic materials. A detailed study on coercivity mechanism can be found in recent papers by Giles and Mansuripur[11] and by Suzuki *et al.*[12] The M_s data measured by the 45° torque technique agree well with those obtained using the VSM. Figure 4(b) shows the measured values of K_u at room temperature, obtained with four different methods. These values of K_u are also listed in Table I. Here we observe the following features: feature 1, $K_u(45°/T)$ and K_u(90°/K) drop in the neighborhood of the compensation composition. Feature 2, for a given sample, $K_u(45°/T)$ is almost always smaller than K_u measured by the Kerr effect or Hall effect techniques. The difference is particularly large near the compensation composition. Feature 3, for FeCo dominant samples ($x<x_c$), $K_u(\mathrm{Rot}/H)$ and $K_u(90°/H)$ decrease as x approaches x_c, while for Tb dominant samples ($x>x_c$), they increase as x approaches x_c, indicating a discontinuous jump in K_u at the compensation point.

In studying the above samples, we also measured M_s, H_c, K_u as functions of temperature T. Figures 5(a) and 5(b) show $M_s(T)$, $H_c(T)$ in the temperature range from −175 °C to +200 °C. Figure 5(c) shows $K_u(T)$ obtained with the "rotating field/Hall effect" technique from room

TABLE I. Measured values of H_c, M_s, and K_u for four $Tb_x(FeCo)_{1-x}$ samples with thickness 800 Å; H_c unit is kOe, M_s unit is emu/cc, and K_u unit is 10^6 erg/cc.

Measured parameter	Technique	$x=20.3\%$	$x=21.4\%$	$x=24.9\%$	$x=26.4\%$
H_c	Hall effect	6.5	8.9	7.3	4.4
M_s	VSM	103	59	71	109
M_s	45° torque	99	50	70	110
$K_u(45°/T)$	45° torque	3.30	0.96	2.9	5.00
K_u(Rot/H)	Rotating Hall	3.72	3.67	5.84	4.48
K_u(90°/H)	In-plane Hall	4.82	2.94	5.71	5.62
K_u(90°/K)	In-plane Kerr	3.14	2.61	4.52	5.58

temperature to 125 °C. Feature 3 as mentioned above can be clearly seen in Fig. 5(c). That is, the $Tb_{24.9}(FeCo)_{73.6}$ sample, which is nearest to the compensation composition with RE dominant in the temperature range of 25–75 °C [cf. Fig. 5(a)], exhibits the largest K_u. The $Tb_{21.4}(FeCo)_{78.6}$ sample, which is nearest to the compensation composition with TM dominant in the ranges of 25–100 °C [cf. Fig. 5(a)], shows the smallest K_u. At 125 °C this sample is far away from the compensation point and does not show the smallest K_u any more.

In order to compare the "45° field/Hall effect" technique with other techniques, we remeasured the four $Tb_x(FeCo)_{1-x}$ samples nine months after the above measurements. This time we used the VSM to measure M_s and used the "in-plane field/Hall effect," "45° field/Hall effect" and "in-plane field/Kerr effect" techniques to measure K_u. The measured data are presented in Table II. One can see that the M_s values deviate slightly from the previous measurements, but the values of K_u and H_c drop significantly. We believe that these changes are due to structural relaxation, because a small change of atomic positions does not affect the magnetic moment, but it can severely affect the anisotropy. In Table II we see that $K_u(90°/K)$ still shows feature 1 and $K_u(90°/H)$ still shows feature 3. Most importantly, we find a new feature: feature 4, $K_u(45°/H)$ is usually greater than $K_u(90°/H)$. The origin of the four features will be explained in Sec. IV by considering the canting between the RE and TM subnetwork magnetizations.

To compare the techniques for single subnetwork ferromagnetic samples (where canting is absent), we investigated two sputtered Co(3 Å)/Pt(10 Å) thin film samples. The 234-Å-thick film was deposited on a silicon substrate, and the 260-Å-thick film was deposited on a glass substrate. Table III summarizes the measured data of M_s using VSM and torque magnetometry and the values of K_u determined with the various techniques. We see that all the different techniques agree very well with each other. For the 260-Å-thick sample we measured $K_u(T)$, $M_s(T)$, $H_c(T)$, and $\theta_k(T)$ in the temperature range from −175 °C

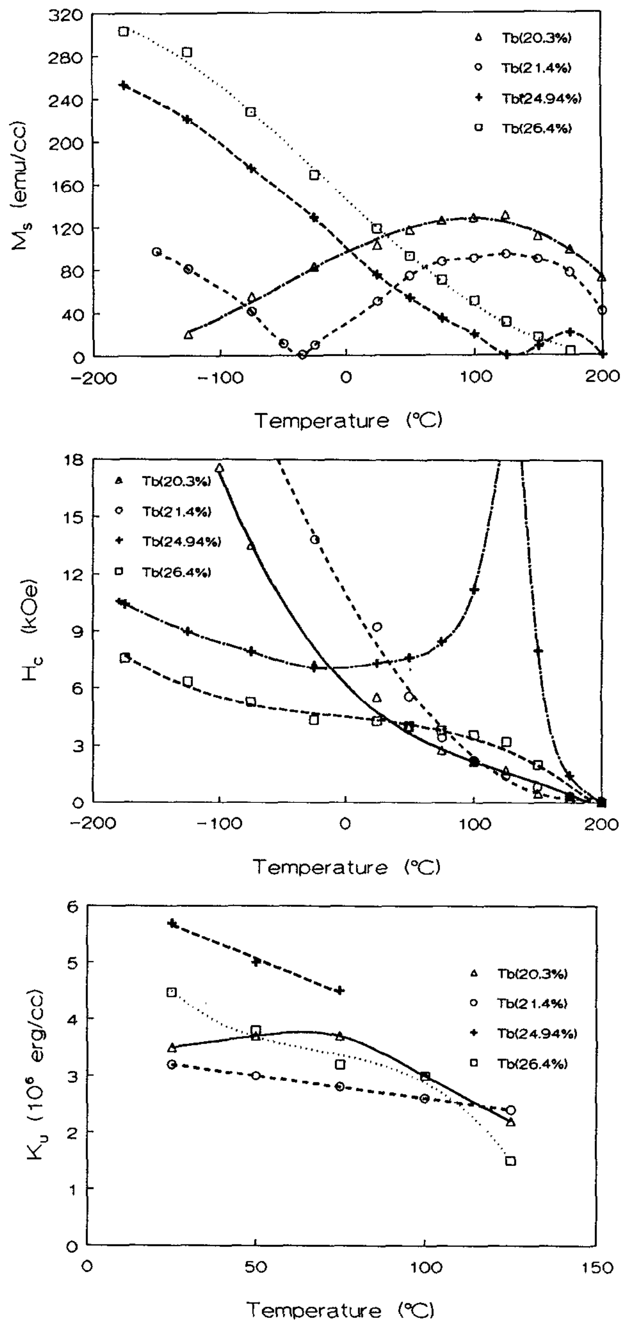

FIG. 5. Temperature dependence of (a) M_s, (b) H_c, and (c) K_u for the four $Tb_x(FeCo)_{1-x}$ samples. M_s was obtained with a VSM, and K_u with the rotating field/Hall effect technique.

to +125 °C. The results are shown in Fig. 6. The two curves of K_u were obtained using the Hall effect/in-plane field and the Kerr effect/in-plane field techniques. Unlike the $Tb_x(FeCo)_{1-x}$ samples, the values measured by the Kerr effect technique (using a wavelength of 632 nm) are also very close to the Hall effect measurements. The reason may be that the Co/Pt samples are much thinner than the $Tb_x(FeCo)_{1-x}$ samples, so that the incident light can go through the whole thickness and the Kerr signal thus gives the bulk value of K_u, as is the case with the Hall effect measurements. Another reason could be that, in contrast to the $Tb_x(FeCo)_{1-x}$ samples where the RE and TM con-

TABLE II. Remeasured values of H_c, M_s, and K_u for four $Tb_x(FeCo)_{1-x}$ samples with thickness 800 Å. H_c unit is kOe, M_s unit is emu/cc, and K_u unit is 10^6 erg/cc.

Measured parameter	Technique	x=20.3%	x=21.4%	x=24.9%	x=26.4%
H_c	Hall effect	4.3	7.4	6.3	3.5
M_s	VSM	100.3	51.4	67.5	108.8
K_u(45°/H)	45° Hall	3.72	2.66	3.27	3.81
K_u(90°/H)	In-plane Hall	2.97	2.12	3.47	2.76
K_u(90° K)	In-plane Kerr	2.77	1.92	2.73	3.34

tribute to the Kerr effect and Hall effect in different proportions, both Kerr and Hall signal are contributed by the same magnetic subnetwork in the Co/Pt samples.

IV. THE CANTING MODEL EXPLANATION

It should be emphasized that, in all the aforementioned techniques, K_u is extracted from the experimental data on the basis of the Stoner–Wohlfarth model. This treatment is only suitable for the coherent rotation of magnetization. If the coherent rotation were the case, K_u should not have depended on the technique. It is also worth pointing out that the drop in K_u near the compensation point is only *apparent*, i.e., it does not correspond to a decrease of the anisotropy energy required to bring the subnetwork magnetization to in-plane direction. This nature is also reflected by the fact that the width and the depth of the drop depend on the measurement techniques.

In this section we show that the four features observed for the $Tb_x(FeCo)_{1-x}$ samples originate from the canting between the RE and TM subnetwork magnetizations. The canting model was first proposed by Rinaldi and Pareti in 1979.[13] They pointed out that in RE-TM compounds the exchange coupling is not strong enough to force the two subnetworks into complete alignment. Based on this concept, Sarkis and Callen showed that for ferrimagnetic RE-TM alloys the canting can lead to an apparent drop of anisotropy constant (measured by torque) near the compensation point.[14] This apparent drop of K_u was also observed by Takagi *et al.*[15] and Hellman *et al.*,[16] and discussed recently by Hellman *et al.*[17] The aim of this section is to study the influence of the canting on the anisotropy constant measured by the techniques based on the Hall and Kerr effects.

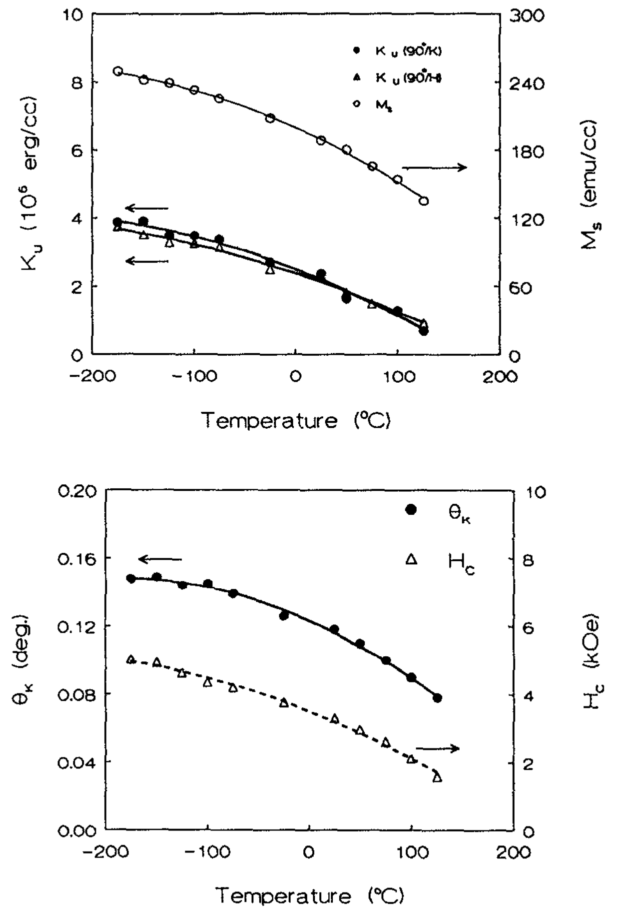

FIG. 6. Temperature dependence of (a) K_u and M_s, (b) θ_k and H_c for the 260-Å-thick Co(3 Å)/Pt(10 Å) sample. The values of K_u marked by ● and Δ were obtained with the in-plane field/Kerr effect and in-plane field/Hall effect techniques, respectively.

The canting model takes into account the individual directions of the subnetwork magnetizations M_R for RE and M_T for TM, see Fig. 7(a). Based on this model it becomes clear why the torque, Hall effect, and Kerr effect techniques give different K_u, because the signal comes from different sources. The measured torque is associated with the net magnetization of the RE and TM subnetworks; the Hall effect is contributed by the TM subnetwork magnetization; and the Kerr effect is mainly contributed by the TM subnetwork, but a small part of the signal also comes from the RE subnetwork, depending on the laser wavelength.

In torque measurement, the reason why a small canting (usually on the order of 1°) can cause a large discrepancy in K_u can be easily explained as follows: Consider the

TABLE III. Comparison between two Co(3 Å)/Pt(10 Å) samples in terms of their M_s values obtained with VSM and TM, and in terms of K_u values obtained with five different techniques. M_s unit is emu/cc, and K_u unit is 10^6 erg/cc. (data obtained at the room temperature).

Thickness (Å)	M_s (VSM)	M_s (45°/T)	K_u (Rot/H)	K_u (90°/H)	K_u (90°/K)	K_u (45°/H)	K_u (45°/T)
234	298	284	5.20	5.18	5.03	5.28	6.41
260	188	183	2.30	2.29	2.38	2.30	2.85

direction Θ of the net magnetization **M** under an external field. In the SW model, Θ is directly related to K_u, i.e., for a given field a smaller Θ implies a larger K_u. However, when $\delta \neq 0$ and $M_R \simeq M_T$, Θ can be very large even though δ, Θ_R, and Θ_T are all very small, see Fig. 7(a). Obviously, this large Θ is not a result of small K_u, but a result of the canting near compensation. Therefore, using the SW model to treat the data of Θ would lead to an *apparent* drop in K_u. Far away from the compensation, the small canting only causes a slight tilt of **M** from the subnetwork magnetizations, see Fig. 7(b), and both the Stoner–Wohlfarth model and the canting model give the same result for K_u. In the following we discuss the canting model in some detail.

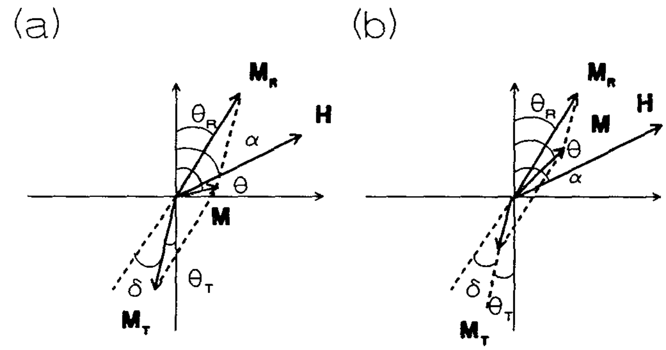

FIG. 7. Schematic diagram showing how the canting between RE and TM subnetworks causes the apparent drop of K_u near compensation. (a) near compensation Θ can be large even if Θ_R, Θ_T, and δ are small ($\delta \neq 0$). (b) Far away from compensation, **M** is almost parallel to the major subnetwork magnetizations and Θ is small.

Let us first study the RE-dominant case (i.e., $M_R > M_T$) shown in Fig. 7(a). In terms of M_R and M_T, and the subnetwork anisotropy constants K_R and K_T, the total energy is written

$$\begin{aligned} E_{\text{tot}} &= H[M_R \cos(\alpha-\Theta_R) - M_T \cos(\alpha-\Theta_T)] \\ &\quad + [K_R \sin^2\Theta_R + K_T \sin^2\Theta_T] \\ &\quad + 2\pi(M_R \cos\Theta_R - M_T \cos\Theta_T)^2 \\ &\quad - \lambda M_R M_T \cos(\Theta_R - \Theta_T). \end{aligned} \tag{3}$$

Here the first three terms are the external, anisotropy, and demagnetizing energy density. The last term is the exchange coupling energy density between RE and TM subnetworks. By calculating the exchange energy between RE and TM atoms per unit volume, one can show that the dimensionless coupling constant λ is given by

$$\lambda = \frac{2Z|J_{\text{RE-TM}}|}{N g_{\text{RE}}\, g_{\text{TM}} \mu_B^2}, \tag{4}$$

where Z is the average coordination number (number of nearest neighbor atoms), $2J_{\text{RE-TM}}$ the exchange energy per RE-TM pair, N the total atomic number density, g_{RE} and g_{TM} the gyromagnetic factor, and $\mu_B(=9.27\times10^{-21}$ emu) the Bohr magneton. The various numbers for a specific RE-TM material can be found in Ref. 18. For $\text{Tb}_x(\text{FeCo})_{1-x}$, we have $Z=12$, $J_{\text{RE-TM}} = -10^{-15}$ erg, $g_{\text{RE}} = 1.5$, $g_{\text{TM}} = 2$. Thus, using $N = 5\times10^{22}$ cm^{-3}, we have $\lambda \simeq 1800$. It is worth pointing out that λ is independent of temperature and composition within the framework of the mean-field theory. The temperature and composition dependence of the exchange energy $(-\lambda \mathbf{M}_R \cdot \mathbf{M}_T)$ are contained in $\mathbf{M}_R$ and $\mathbf{M}_T$.

The solution for Θ_R and Θ_T of Eq. (3) can be found by minimizing E_{tot} with respect to Θ_R and Θ_T. Near compensation, both Θ_R and Θ_T are small (e.g., $<10°$), and Eq. (3) can be solved analytically by neglecting $O(\Theta_R^2)$ and $O(\Theta_T^2)$ terms. Defining the subnetwork anisotropy fields $H_R = 2K_R/M_R$ and $H_T = 2K_T/M_T$, the solution of Eq. (3) in the case of $M_R > M_T$ can be written as follows:

$$\begin{aligned} \Theta_R &= \frac{H \sin\alpha(\lambda M_s + H_T - H\cos\alpha)}{\lambda(2K_R + 2K_T - 2\pi M_s^2 + HM_s\cos\alpha) + (H_T - H\cos\alpha + 4\pi M_s)(H_R + H\cos\alpha - 4\pi M_s)} \\ \Theta_T &= \frac{H \sin\alpha(\lambda M_s - H_R - H\cos\alpha)}{\lambda(2K_R + 2K_T - 2\pi M_s^2 + HM_s\cos\alpha) + (H_T - H\cos\alpha + 4\pi M_s)(H_R + H\cos\alpha - 4\pi M_s)}. \end{aligned} \tag{5}$$

Now we discuss the behavior of K_u (as defined in the SW model) based on the canting model. The numerical results are plotted in Fig. 8. Let us first discuss the torque measurement. The torque L is given by $L = HM\sin(\alpha-\Theta)$. From Fig. 7 we have $M\sin\Theta = M_R\sin\Theta_R - M_T\sin\Theta_T$ and $M\cos\Theta = M_R\sin\Theta_R - M_T\sin\Theta_T$. Therefore, L is written as

$$\begin{aligned} L &= H[\cos\alpha(M_R\sin\Theta_R - M_T\sin\Theta_T) \\ &\quad - \sin\alpha(M_R\cos\Theta_R - M_T\cos\Theta_T)]. \end{aligned} \tag{6}$$

From Eqs. (5) and (6) we can find $(L/H)^2$ as a function of L for $\alpha=45°$, which is generally a curve (not a straight line as predicted by the SW model) due to the canting, as observed in our torque measurement. Using a straight line $(L/H)^2 = a - b\,L$ to match this curve by the least squares method, we find the coefficients a and b, and K_u is then given by $K_u = 4\pi a + a/b$, see Sec. II A. Equations (3), (5), and (6) are for $M_R > M_T$, but the solution for the case $M_R < M_T$ can be obtained simply by making the change $R \leftrightarrow T$ in the subscripts.

In the Hall/Kerr effect measurements, the signal is known to be mainly contributed by the TM. In the calcu-

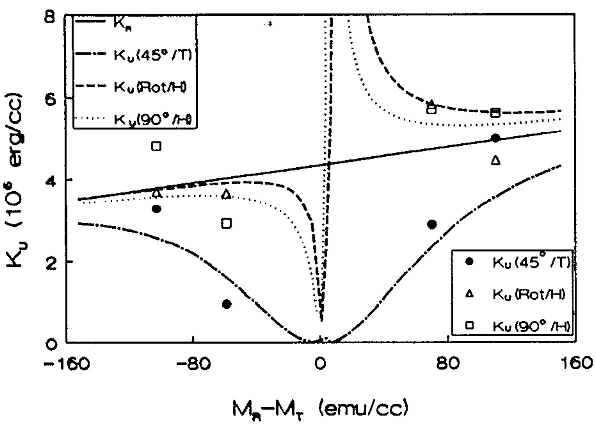

FIG. 8. The calculated K_u as a function of (M_R-M_T). The solid line is the subnetwork (physical) anisotropy constant K_R. The dash-dotted curve is for $K_u(45°/T)$. The dashed curve corresponds to K_u(Rot/H), which is actually equal to $K_u(45°/H)$ (not shown), and the dotted curve corresponds to $K_u(90°/H)$. The corresponding experimental data are also given. The four features observed in the experiments are clearly reproduced by the canting model.

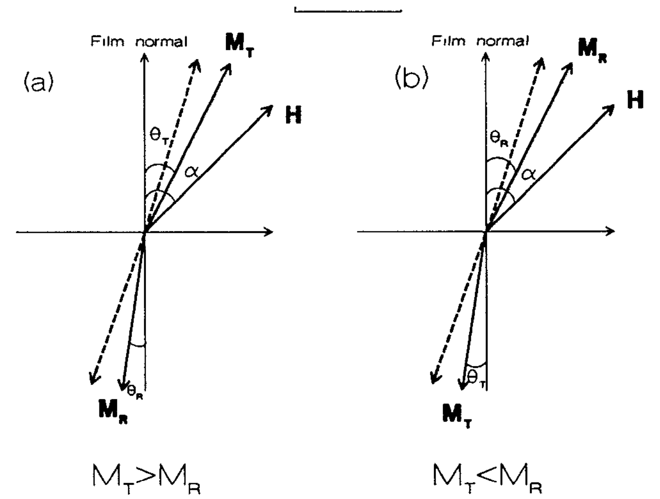

FIG. 9. Schematic explanation of the dip and the peak in K_u measured by the Hall effect techniques. The dashed arrows represent the subnetwork magnetizations for infinite coupling, while the solid arrows are for finite coupling. (a) In the TM-dominant case, M_T is more tilted than the dashed arrow, thus leading to the dip. (b) In the RE-dominant case, M_T is less tilted than the dashed arrow, which causes the peak.

lations we have assumed all the measured signal is contributed by the TM subnetwork. In extracting K_u from the experimental data based on the SW model, this assumption means Θ in the SW model is considered to be $|\Theta_T|$, where we have assumed Θ to be positive because it is deduced from $\cos \Theta_T$ in the Hall/Kerr measurement. The theoretical K_u for the Hall/Kerr techniques is calculated in the following way. For a given series of field strength and angle $\{H_i,\alpha_i\}$, which simulates a specific technique (45°, in-plane or rotating field), we first use the canting model solution Eq. (5) to obtain a series of data points $\Theta_{\text{cant},i} = |\Theta_T(H_i,\alpha_i)|$. On the other hand, we also find a series of data points $\Theta_{\text{sw},i} = \Theta(H_i,\alpha_i)$ from the SW model for given $M_s = |M_R-M_T|$ and K_u (unknown). The error between the two series of data $\Sigma_i\ (\Theta_{\text{cant},i} - \Theta_{\text{sw},i})^2$ is a function of K_u. We can thus find K_u by minimizing the error.

To numerically simulate our measurements, we allowed the atomic percentage of the RE element, X_R, to vary from 0.19 to 0.27, but kept the temperature at room temperature. Based on the room temperature experimental data of M_s, we use $M_R = 2644X_R$ emu cm^{-3}, $M_T = 799\ (1-X_R)$ emu cm^{-3}. Thus, for the (FeCo)-dominant sample $Tb_{20.3}(FeCo)_{79.7}$ we have $M_s = M_T - M_R = 100$ emu cm^{-3}, for the Tb-dominant sample $Tb_{26.4}(FeCo)_{73.6}$ we have $M_s = M_R - M_T = 110$ emu cm^{-3}. The room temperature compensation composition is $x_c = 23.2\%$, at which $M_R = M_T = 613$ emu cm^{-3}. K_T is assumed to be zero. K_R is chosen to be equal to $2.05\times 10^7 X_R$ erg cm^{-3}, which is the only parameter that we adjust to match the experimental data. We use the mean-field theory result for the exchange coupling constant, i.e., $\lambda = 1800$.

The calculated K_u vs (M_R-M_T) for the torque and Hall effect techniques are shown in Fig. 8. The solid line is the subnetwork anisotropy constant K_R, which is the intrinsic physical property of the material. The calculated $K_u(45°/T)$, $K_u(\text{Rot}/H)$, and $K_u(90°/H)$ are represented by the dot-dashed curve, the dashed curve, and the dotted curve, respectively. The calculated $K_u(45°/H)$ (not shown) is found to be actually equal to the calculated $K_u(\text{Rot}/H)$. To attempt a quantitative comparison between the calculated and the measured K_u, the experimental data based on the three techniques are also shown in Fig. 8. From this figure we see that the canting model results show all the four features observed in the measurements as we mentioned in Sec. III. That is, $K_u(45°/T)$ drops near compensation composition (feature 1); $K_u(45°/T)$ is smaller than K_u measured by the Hall/Kerr effect techniques (feature 2); near compensation, $K_u(\text{Rot}/H)$ and $K_u(90°/H)$ exhibit a dip for TM-dominant samples and a peak for RE dominant samples (feature 3); $K_u(45°/H) = K_u(\text{Rot}/H) > K_u(90°/H)$ (feature 4). We have thus shown how the canting causes the various apparent behaviors of K_u near the compensation point. These features are found to be general in the canting model, as far as the parameters used are of the correct order of magnitude as listed below Eq. (4).

The physics of the dip and the peak appearing near the compensation point can be explained with the help of Fig. 9. The dashed arrows represent the magnetization in the case of infinite coupling. In reality, the coupling constant is finite, which has the following consequences: In the case of $M_T > M_R$, M_T (which provides the main part of the Hall signal) is more tilted than the dashed arrow, while the opposite is true in the case of $M_R > M_T$. This leads to an underestimate of K_u for the TM-dominant case and an overestimate for the RE-dominant case.

It is important to notice that the extent of the apparent deviations is much different for the various techniques. In the torque technique the apparent dip is very wide and starts at $|M_R-M_T| \simeq 100$ emu cm^{-3}, see Fig. 8. In the Hall/Kerr effect case the width of the apparent dip and peak depends on whether the RE contributes to the signal.

Let S_{RE} be the percentage contributed by RE to the total measured signal. It is generally believed that $S_{RE} < 50\%$, as evidenced by the fact that the hysteresis loop switches sign as the sample crosses the compensation point. Our simulations (not shown) show that both dip and peak are very narrow for $S_{RE}=0$; they become broader with increasing S_{RE} (but even for $S_{RE}=40\%$ they are still much narrower than the torque case); and in the limiting case of $S_{RE}=50\%$ the peak disappears and the dip becomes very wide (similar to torque). To match the Hall effect experimental data $K_u(\mathrm{Rot}/H)$ and $K_u(90°/H)$, we have used $S_{RE}=0$ (see Fig. 8). The fact that $K_u(90°/\mathrm{K})$ do not show the peak means that S_{RE} for Kerr effect is larger than zero. This result (i.e., $S_{RE}=0$ for Hall effect and $S_{RE}>0$ for Kerr effect) is consistent with the mechanisms for the extraordinary Hall effect and the magneto-optical Kerr effect.[19]

V. CONCLUDING REMARKS

In this article we have experimentally demonstrated and theoretically shown that the so-called intrinsic magnetic anisotropy constant K_u for ferrimagnetic RE-TM materials as defined in the SW model is dependent on the measurement technique. Five different techniques based on torque, Hall effect, and Kerr effect are discussed. The main difference among the techniques comes from the fact that they measure different combinations of the RE and TM subnetwork magnetizations which are not strictly antiparallel, as it is taken for granted in most cases. Due to the canting between RE and TM subnetworks, all the techniques produce some unexpected behavior in K_u. The torque technique produces a wide and deep apparent dip. The Hall effect techniques produce a much narrower dip for the TM-dominant case and a narrow peak for the RE-dominant case. The Kerr effect technique is much like Hall effect technique, although it does not produce the apparent peak. In this regard, the Hall and Kerr effect techniques are more applicable for ferrimagnetic RE-TM samples. However, for a complete characterization of a RE-TM sample, one must know all the subnetwork properties including M_R, M_T, K_R, K_T, and λ, which can only be determined when both $\Theta_R(\mathbf{H},\alpha)$ and $\Theta_T(\mathbf{H},\alpha)$ are measured. None of the techniques discussed in this article is capable on its own to provide complete information on both Θ_R and Θ_T. To achieve this goal, one has to combine two different techniques, for example the torque and the Hall effect techniques, in the measurements.

[1] E. C. Stoner and E. P. Wohlfarth, Philos. Trans. R. Soc. A **240**, 599 (1948).

[2] S. Chikazumi and S. H. Charap, *Physics of Magnetism* (Krieger, Malabar, FL, 1964).

[3] H. Miyajima, K. Sato, and T. Mizoguchi, J. Appl. Phys. **47**, 4669 (1976).

[4] T. Wielinga, J. Appl. Phys. **50**, 4888 (1979).

[5] K. Ishibashi, Y. Uchiyama, U. Hwang, and T. Suzuki, J. Appl. Phys. **63**, 2914 (1988).

[6] M. Tejedor, A. Fernandez, and B. Hernando, IEEE Trans. Mag. **MAG-24**, 1995 (1988).

[7] P. Wolniansky, S. Chase, R. Rosenvold, M. Ruane, and M. Mansuripur, J. Appl. Phys. **60**, 346 (1986).

[8] R. A. Hajjar, F. L. Zhou, and M. Mansuripur, J. Appl. Phys. **67**, 5328 (1990).

[9] R. A. Hajjar, T. H. Wu, and M. Mansuripur, J. Appl. Phys. **71**, 813 (1992).

[10] Hong Fu, R. Giles, M. Mansuripur, and G. Patterson, Computers in Physics (to be published).

[11] R. Giles and M. Mansuripur, Computers in Physics, March/April, 204 (1991).

[12] T. Suzuki, H. Notarys, D. Dobbertin, and C-J. Lin, IEEE Trans. Mag. (to be published).

[13] S. Rinaldi and L. Pareti, J. Appl. Phys. **50**, 7719 (1979).

[14] A. Sarkis and E. Callen, Phys. Rev. B **26**, 3870 (1982).

[15] H. Takagi, S. Tsunashima, S. Uchiyama, and T. Fujii, J. Appl. Phys. **50**, 1642 (1979).

[16] F. Hellman, R. B. van Dover, S. Nakahara, and E. M. Gyorgy, Phys. Rev. B **35**, 591 (1989).

[17] F. Hellman, Appl. Phys. Lett. **59**, 2757 (1991).

[18] M. Mansuripur and M. F. Ruane, IEEE Trans. Mag. **MAG-22**, 33 (1986).

[19] Hong Fu, A. F. Zhou, and M. Mansuripur (unpublished).